



Electronic Goos-Hänchen shifts in phosphorene

Parisa Majari ^{a,*}, Gerardo G. Naumis ^b

^a Instituto de Ciencias Físicas, Universidad Nacional Autónoma de México (UNAM), Cuernavaca 62210, Morelos, Mexico

^b Depto. de Sistemas Complejos, Instituto de Física, Universidad Nacional Autónoma de México (UNAM), Apdo. Postal 20-364, 01000, CDMX, Mexico

ARTICLE INFO

Keywords:

Goos-Hanchen shifts
Phosphorene
Klein tunneling

ABSTRACT

The total internal reflection of a light beam on a surface in classical optics leads to a lateral displacement along the interface plane. This is known as the Goos-Hänchen (G-H) and usually is very weak. Two-dimensional materials are suitable platforms to generate electronic analogies of the G-H shifts. Here, a theoretical study is performed to evaluate the possibility of increasing the magnitude of the G-H effect in phosphorene. In particular, the G-H shifts and the transmission coefficient are studied for electrons crossing different kinds of potential barriers in phosphorene. Here, a transfer matrix approach is used taking into account current conservation and the problem of non-Hermiticity of the envelope effective equation for sharp boundaries. The obtained results show that the G-H shifts are strongly dependent on the type of barrier and incident angle, yet are suitable to be detected as it turns out to be bigger than in graphene.

1. Introduction

Novel two-dimensional materials have proved to be powerful tools in nanoelectronics due to their unique optical, mechanical, electronic, and thermal properties [1–10]. The distinct characteristics exhibited by 2D materials have led to their application in a wide range of optical devices, including optical detectors and modulators [11,12]. Moreover, Janus meta-structures can be formed by combining different two-dimensional (2D) materials, tailored to specific applications in physics [13–15]. Furthermore, 2D materials such as graphene, transition metal dichalcogenides (TMDs), and black phosphorus, can be used for magnetic sensors due to their unique properties, which can enhance the sensitivity of such sensors [16,17]. Among these two-dimensional materials, graphene has generated considerable interest due to its high bipolar mobility, exceptional conductivity, and mechanical strength [18–24]. Despite these properties, graphene is a gapless semiconductor, and to be used in electronic devices, it is essential to generate a distinct band gap in its electronic energy structure [25–29]. As a band gap is essential for electronic applications, a single or few-layer form of black phosphorus with an anisotropic orthorhombic structure is one of the most promising materials [30–32].

Black phosphorus is a layered allotrope of phosphorus that is derived from bulk black phosphorus. Phosphorene exhibits anisotropic properties due to its crystal structure, which consists of a puckered honeycomb lattice of phosphorus atoms [33–35]. In this lattice, the electronic and optical properties are governed by its energy bandgap and crystal lattice direction that has a bilayer and puckered configuration along the zigzag and armchair directions respectively.

Considering the bandgap, blue phosphorene has a wider band gap than black phosphorene [36,37]. In this paper, we consider black phosphorene as it has a moderate band gap and good electrical conductivity which makes it a candidate for electronic and optoelectronic applications. The band gap in phosphorene generally decreases as the number of layers increases. Specifically, single-layer phosphorene exhibits a larger band gap (about 1.8 eV) when compared to bilayer or few-layer phosphorene [38–40]. On the other hand, the influence of strain on the bandgap of phosphorene varies depending on the type of strain, such as uniaxial and biaxial, as well as on the direction and magnitude of the applied strain [41]. Moreover, the application of an electric field can significantly influence the bandgap of phosphorene as it causes a shift in the energy levels of electrons and holes [42,43]. The band gap of phosphorene can be influenced or regulated through a range of methods and techniques, including adjusting the number of layers, employing strain engineering, applying electric fields, and utilizing chemical doping [44–49].

On the other hand, materials with wider band gaps tend to have higher dielectric constants. Phosphorene's dielectric constant varies along distinct crystallographic directions owing to its anisotropic nature. The dielectric tensor element along the armchair direction is represented by ϵ_{xx} while along the zigzag direction, it is represented by ϵ_{yy} . The off-diagonal elements of the dielectric constant tensor (ϵ_{xy} , ϵ_{yx}) are indicative of the coupling between these two directions. The dielectric constant is influenced by factors such as crystal orientation, strain, and the presence of external fields. The density functional theory

* Corresponding author.

E-mail addresses: majari@icf.unam.mx (P. Majari), naumis@fisica.unam.mx (G.G. Naumis).

(DFT) is a well-known method for obtaining the dielectric properties of phosphorene and it has been widely used in previous studies [50–52].

Many papers have been recently devoted to study and control quantum transport in phosphorene, especially concerning the experimental realization of the Klein tunneling (KT) [53–55]. The KT is a quantum mechanical relativistic effect where the electron is transmitted with probability one through a potential barrier junction for normal incidence [53,54,56–58]. A recent theoretical work (see Ref. [59]) studied the transmission of electrons in phosphorene through a step potential. It was shown that transmission in the armchair junction is perfect for normal incidence.

Of important interest is the mimicking of optical effects using electrons propagating in two dimensional materials [55,56,60]. This includes the possibility of using different kinds of degrees of freedom. We can cite as an example the use of Kekulé-induced valley birefringence in graphene [61].

The G-H shift is one of the less explored electronic analogs of an optical effect. In classical optics, the GH shift is a lateral displacement of a light beam along an interface. This is observed when there is a total internal reflection of the beam on the surface due to the interference of the different components of a wave packet. 2D materials, negative refraction index materials, and epsilon-near-zero (ENZ) materials have been used for exploring GH shifts [62–70]. However, it is important to have a G-H effect large enough to be observed experimentally, and consequently, graphene has been proposed as a suitable candidate for engineering G-H shifts [71]. This kind of shift has been verified in a number of experiments by using different methods such as a weak measurement technique and the beam splitter scanning method [72, 73].

Our interest in phosphorene also arises due to the uniqueness of the electronic G-H shift obtained from its distinctive electronic and optical properties. Phosphorene demonstrates anisotropic behavior in both its electronic and optical properties. Electronic G-H shifts provide the capability to control electron waves at the nanoscale. This level of control is essential in nanoelectronic devices which can lead to improved resolution in electron beam lithography and imaging techniques [74]. Moreover, as phosphorene has the capability to create quantum dots, it could potentially contribute to quantum computing where these quantum dots function as qubits. Control and manipulation of G-H shifts play an important role in quantum computing and quantum information processing technologies.

Here we discuss the effect of a single and double potential barriers on the transport properties of phosphorene. Also, transport along the armchair direction of phosphorene is faster than in the zigzag direction. As high electron velocities are critical for the advancement of future electronic devices, we will study the transport properties of phosphorene along the armchair direction [75,76]. Notice that one can also study periodic barriers and randomly distributed atomic defects. However, here we restrict our attention to few barriers as a first step. When adding more barriers usually one requires the understanding of resonances and effects with few barriers and thus the present work can serve as a starting point. One important aspect of why doing such a study is that the electrons and holes in phosphorene behave as nonrelativistic and relativistic particles along zigzag and armchair directions respectively [77]. In graphene, electrons always behave as effective relativistic particles. The second aspect is to study the possibility of an enhancement of the G-H effect due to the strong anisotropy. We note that the Hamiltonian of phosphorene is a combination of the Dirac and Schrodinger models along the armchair and zigzag direction, respectively. In the case of the zigzag junction, we have both propagating and evanescent modes due to the existence of four eigenstates in the Hamiltonian while in the case of the armchair junction, only propagating modes are included. We note that the case of zigzag junction is equivalent to graphene under strong uniaxial strain. Despite this fact, in a previous work concerning the G-H effect in graphene with

uniaxial strain, the evanescent modes were neglected [78]. Our theoretical proposal can be experimentally implemented in phosphorene by using the beam splitter scanning method [72,73], and also in analog systems that emulate the Hamiltonian of phosphorene, like in arrays of dielectric resonators or by using engineered periodic optical structures created with waveguide arrays [3,79].

This paper is organized as follows: In Section 2 we describe the theoretical framework to evaluate the tunneling of particles through armchair junctions in phosphorene and the possibility of increasing the magnitude of the G-H effect. Section 3 presents the main results of this work, including the influence of different kinds of barriers and energy of the incident particle on the G-H shifts and transport properties of phosphorene. Finally in Section 4 we make some concluding remarks.

2. Goos Hnchen like shifts in phosphorene along the armchair direction

In this section we will study the presence of a G-H-like shift and Klein tunneling in phosphorene with armchair junctions. The effective low-energy Hamiltonian of phosphorene is written as [59],

$$H = \left(\frac{E_g}{2} + \frac{\hbar^2 k_x^2}{2m^*} \right) \sigma_x + \hbar v_y k_y \sigma_y, \quad (1)$$

where $m^* = 1.42m_e$ is the effective mass and $v_y = 5.6 \times 10^5$ m/s is the velocity along the armchair direction. As seen in Fig. 1, the index x denotes an axis along the zigzag direction while the y -axis is directed along the armchair direction. The operators σ_x and σ_y are the usual Pauli matrices. The band gap of phosphorene is determined by the parameter E_g [59]. Note that electrons in single-layer graphene are characterized by massless relativistic fermions. The dynamics of these electrons are described by a Dirac-like Hamiltonian $H = v_f \boldsymbol{\sigma} \cdot \mathbf{p}$ where $\boldsymbol{\sigma} = (\sigma_x, \sigma_y)$ are the Pauli matrices and $v_f \simeq 9 \times 10^5$ m/s is the Fermi velocity. Notice that the Hamiltonian given by Eq. (1) is equivalent to a graphene Hamiltonian under very strong uniaxial strain [48,80]. In fact, Eq. (1) indicates that the energy dispersion is quadratic in the x direction and linear in the y direction. Therefore, the Hamiltonian describes two flavors, Dirac-like particles in the y direction and Schrödinger-like particles in the x direction.

As seen in (Fig. 1-a), we will consider a gate voltage that produces a static step potential of height V_0 along the armchair direction,

$$V(y) = \begin{cases} 0 & \text{for } 0 < y, \\ V_0 & \text{otherwise.} \end{cases} \quad (2)$$

Then we will study transport properties through a single, scalar potential barrier of width D (see Fig. 1-b),

$$V(y) = \begin{cases} V_0 & \text{for } 0 \leq y \leq D, \\ 0 & \text{otherwise.} \end{cases} \quad (3)$$

and thereafter a double scalar barrier as seen in see (Fig. 1-c),

$$V(y) = \begin{cases} 0 & \text{for } 0 < y, \\ V_0 & \text{for } 0 \leq y \leq D, \\ 0 & \text{for } D < y < D + L, \\ V_0 & \text{for } D + L \leq y \leq 2D + L, \\ 0 & \text{otherwise.} \end{cases} \quad (4)$$

A recent theoretical work (see Ref. [59]) studied the transmission for a potential step. Here we discuss electrons transmitted through a static square barrier which extends in the region $0 \leq y \leq D$. This is equivalent to study the case seen in (Fig. 1-b). The quantum eigenvalue equation $H\Phi = E\Phi$ admits the following solution for $y < 0$ (region I):

$$\Phi^I = e^{ik_y y} \begin{pmatrix} 1 \\ e^{i\theta k_y} \end{pmatrix} + r e^{-ik_y y} \begin{pmatrix} 1 \\ e^{i\theta - k_y} \end{pmatrix}, \quad (5)$$

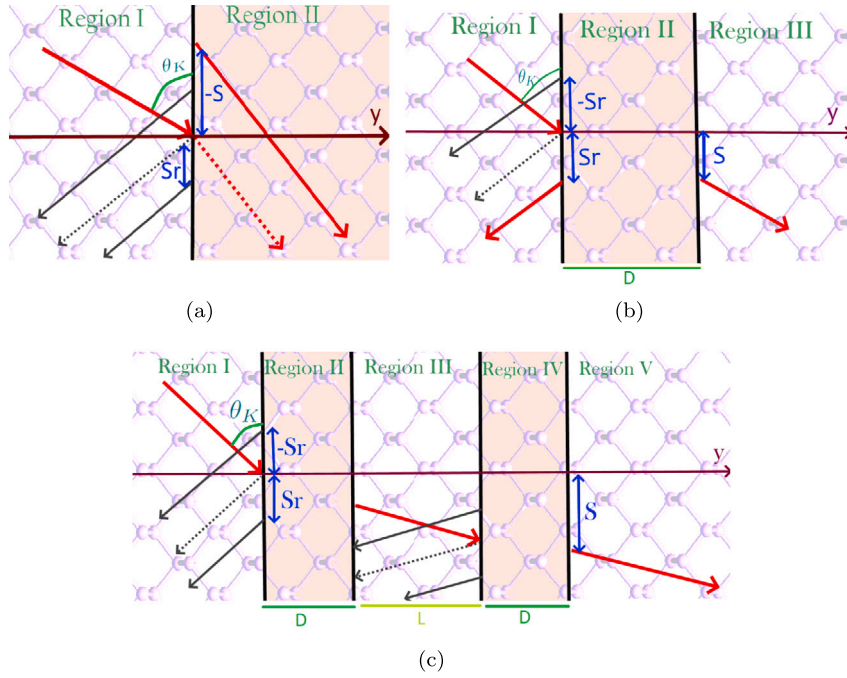


Fig. 1. The G-H shift (S_r) occurs along the interface between incident and reflected particles with incident angle θ_K as they pass through different types of barriers along the armchair direction. a) Step potential, b) single barrier, and c) double barrier. The shade indicate regions where a gate potential is applied. The incidence angle θ_k is indicated, as well as the incident (red arrow to the left), reflected (black arrow), and transmitted (red arrows) electron beams.

where r is the reflection coefficient and,

$$\theta_K \equiv \theta_{k_y} = \arg[(E_g/2 + \hbar^2 k_x^2 / (2m^*)) + i\hbar v_y k_y]. \quad (6)$$

The above expression indicates that at normal incidence ($\theta_K = 90^\circ$), electrons behave like Dirac particles, and near this angle the Dirac term dominates the Schrödinger one. The wavefunction inside the barrier (region II) can be expressed as:

$$\Phi^{II} = A e^{i q_y y} \begin{pmatrix} 1 \\ -e^{i\theta_{q_y}} \end{pmatrix} + B e^{-i q_y y} \begin{pmatrix} 1 \\ -e^{i\theta_{-q_y}} \end{pmatrix}. \quad (7)$$

where A and B are constants that can be determined by the boundary conditions. The y components of the momentum in the different regions are given by:

$$k_y = \left(\frac{1}{v_y \hbar} \right) \sqrt{E^2 - \left(\frac{E_g}{2} + \frac{\hbar^2 k_x^2}{2m^*} \right)^2}, \quad (8a)$$

$$q_y = \left(\frac{1}{v_y \hbar} \right) \sqrt{(E - V_0)^2 - \left(\frac{E_g}{2} + \frac{\hbar^2 k_x^2}{2m^*} \right)^2}. \quad (8b)$$

Similarly, the wavefunction for transmitted electrons in region III reads:

$$\Phi^{III} = t e^{i k_y y} \begin{pmatrix} 1 \\ e^{i\theta_{k_y}} \end{pmatrix}. \quad (9)$$

Here, t is transmission coefficient. Due to the translational invariance along the x direction, momentum is conserved along the x direction, and thus $k_x = q_x$.

As we are dealing with an effective equation deduced from an atomic tight-binding Hamiltonian, we will require the continuity of the wave function at the boundaries between regions and the conservation of current for the envelope wave function [81–83]. In this case, we have the following relation at $y = 0$:

$$\Phi^I(x, 0) = \Xi \Phi^{II}(x, 0) \quad (10)$$

The matrix Ξ should satisfy the condition that the Hamiltonian of the entire system must remain Hermitian and that current must be

conserved along the y -direction. In order to have continuity of the envelope wave function, the following inner product $\langle \Phi^I | H \Phi^{II} \rangle = \langle H \Phi^I | \Phi^{II} \rangle$ have to be satisfied. By inserting this inner product into Eq. (10), we have:

$$\Xi^\dagger \sigma_y \Xi = \sigma_y \quad (11)$$

Furthermore, the matrix Ξ should satisfy the commutation relation $[\tau, \Xi] = 0$, where τ is time-reversal symmetry operator and as shown in Ref. [83], a general type of Ξ can be proposed as follows:

$$\Xi = \gamma_0 \sigma_0 + i(\gamma_x \sigma_x + \gamma_y \sigma_y + \gamma_z \sigma_z) \quad (12)$$

By substituting this general form of Ξ in Eq. (11), and taking into account that Ξ is a Hermitian and unitary ($\Xi \Xi^\dagger = 1$), this matrix can be expressed as:

$$\Xi = \sigma_0, \quad (13)$$

We carry out a similar method for the conservation of current for the envelope wave function at $y = D$. Therefore, in this case, we prove that the current is conserved just by demanding the usual continuity of the wave function as no rotation of pseudospin is produced at the boundary. By satisfying the boundary condition at the interface ($y = 0$), we have:

$$1 + r = A + B, \quad (14a)$$

$$e^{i\theta_{k_y}} + r e^{i\theta_{-k_y}} = -A e^{i\theta_{q_y}} - B e^{i\theta_{-q_y}} \quad (14b)$$

Furthermore, matching the wave function at $y = D$ gives the following system of equations:

$$A e^{i q_y D} + B e^{-i q_y D} = t e^{i k_y D}, \quad (15a)$$

$$-A e^{i q_y D} e^{i\theta_{q_y}} - B e^{-i q_y D} e^{i\theta_{-q_y}} = t e^{i k_y D} e^{i\theta_{k_y}} \quad (15b)$$

The solution of this set of equations can be used to calculate the reflection and transmission coefficients. The reflection coefficient in the case of one static barrier is given by,

$$r = N \frac{-1 + e^{-2i q_y D}}{N - M^* e^{-2i q_y D}}, \quad (16)$$

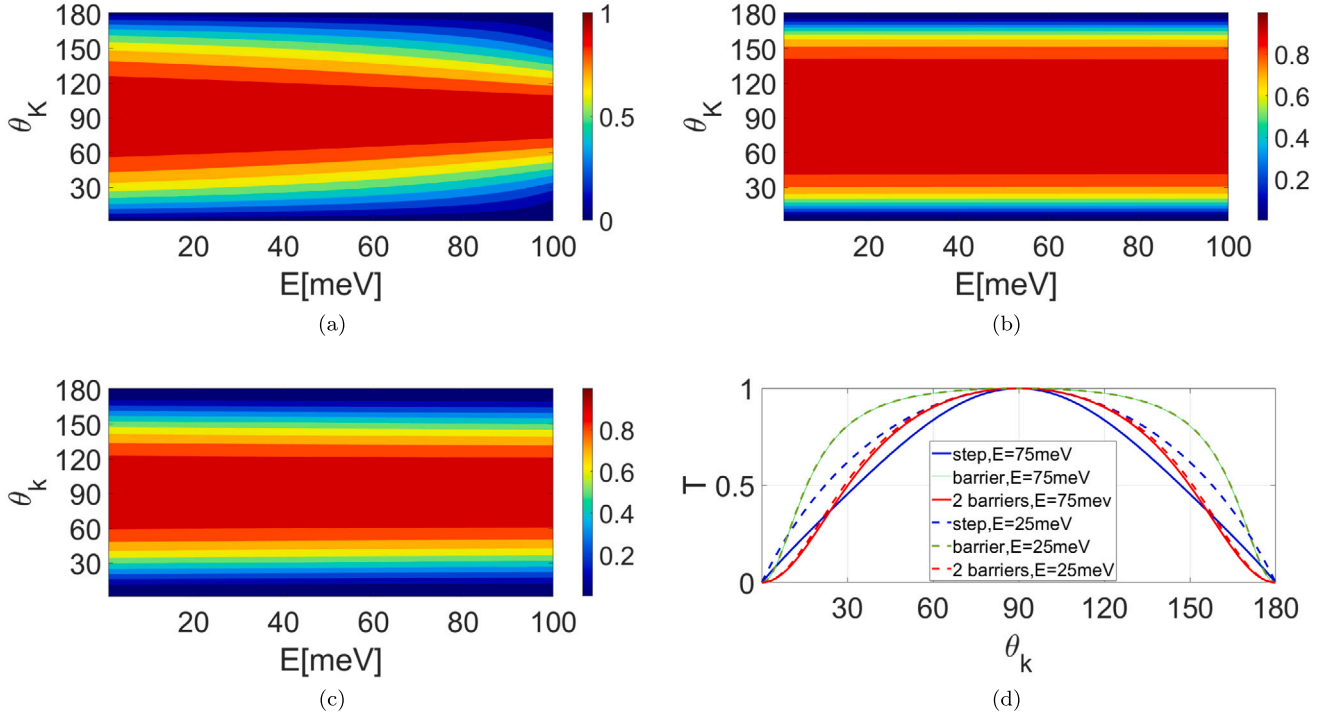


Fig. 2. Transmission probability for armchair junctions with $V_0 = 200$ meV and $E_g = -0.4$ eV for, (a) for a step potential as functions of incidence angle and energy, (b) as a function of the incidence angle and energy for the single potential barrier with width $D = 30$ nm, (c) for a double barrier with a separation distance, $L = 40$ nm, widths $D = 30$ nm. The color bars in Figs (a), (b), and (c) represents the transmission probability. Panel (d) presents the profile of T as a function of the incidence angle for a step potential (blue line), single potential barrier (green line) with width $D = 30$ nm, double potential barriers (red line) with a separation distance, $L = 40$ nm, widths $D = 30$ nm and energy $E = 75$ meV. The dashed lines are the transmission probabilities for the energy $E = 25$ meV.

where the following shorthand notation is used:

$$N = e^{i\theta_{q_y}} + e^{i\theta_{k_y}}, \quad (17)$$

and

$$M = e^{i\theta_{k_y}} + e^{i\theta_{-q_y}}. \quad (18)$$

On the other hand, the transmission coefficient is given by:

$$t = e^{-iD(q_y+k_y)} \frac{(N + rM^*)}{N}. \quad (19)$$

We can rewrite the above transmission coefficient in the following complex form $t = \rho e^{i\varphi}$, with:

$$\varphi = \arctan\left(\frac{W[G(1 - \cos(2q_y D)) - (F - W)\sin(2q_y D)]}{(F - W)[F - W\cos(2q_y D)] + G[G + W\sin(2q_y D)]}\right) - D(q_y + k_y). \quad (20)$$

where,

$$G = 2\sin(\theta_{k_y})[\cos(\theta_{k_y}) + \cos(\theta_{q_y})], \quad W = 2(1 + \cos(\theta_{k_y})\cos(\theta_{q_y}) - \sin(\theta_{k_y})\sin(\theta_{q_y})) \quad (21)$$

and,

$$F = 1 + \cos(\theta_{k_y})^2 - \sin(\theta_{k_y})^2 + 2\cos(\theta_{k_y})\sin(\theta_{q_y}) \quad (22)$$

The dependence on the phase and transmission coefficient on the term $\exp(-2iq_y D)$ demonstrates that the G-H shift is enhanced when there is resonance for transmission at $2q_y D = n\pi$, which allows to have control over the magnitude of the G-H shift. To illustrate this effect, the reader may want to look at Figure (5) of ref [84] as a classical analog of the G-H shift, where sequential decay in rearrangement scattering is studied [85]. Consequently, the G-H shift with respect to the transmission phase shift and parallel wave vector component is

given by [59]:

$$S = -\frac{\partial\varphi}{\partial k_x}. \quad (23)$$

In a similar way, the transmission, reflection, and GH shift can be obtained for the double barrier just by considering each spatial region and corresponding boundaries.

3. Numerical results and discussion

In this section, we calculate the transport properties and G-H shifts in phosphorene with armchair junctions. Fig. 2 presents the transmission coefficient as a function of the energy and incidence angle for the three kinds of barriers seen in Fig. 1. For all energies in the considered range, Fig. 2 shows a perfect transmission for incoming electrons at a normal incidence across a potential step, single and double barriers. This can be further confirmed in Fig. 2 d) where we plot the transmission probability as a function of θ_k for fixed energies. Such perfect transmission is the trademark of the expected Klein effect at normal incidence. Indeed, using definition (8), we have the following condition,

$$\left|1 - \frac{V_0}{E}\right| \geq |\cos(\theta_{k_y})|. \quad (24)$$

Beyond this range, the wave number will be imaginary inside the barriers. Here we chose an energy in the range of $E \leq V_0/2$ in which there are no evanescent waves.

As shown in Fig. 2(a), for large deviations of θ_k from normal incidence and in the case of the potential step, the transmission decreases as energy increases. As can be easily seen from Fig. 2(b) and Fig. 2(c), the transmission probability is almost independent of the energy of the incident particle in the cases of a single and a double barrier. Notice that the transmission coefficient in the case of a single and a double barrier is an exponential function of $q_y D$ [see Eq. (19)]. Thus we expect

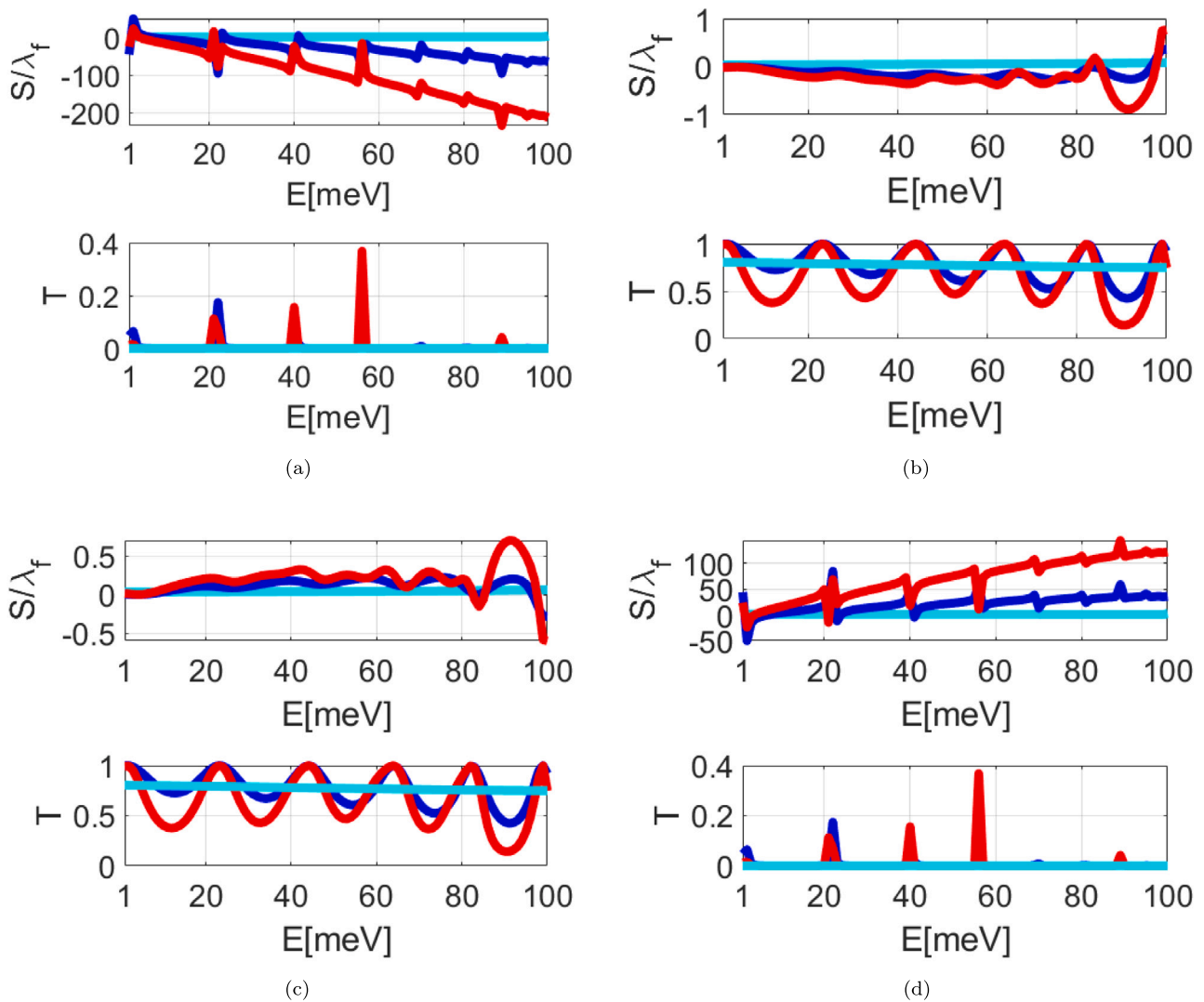


Fig. 3. The transmissions and G-H shifts (S/λ_f) as a function of the energy (where $\lambda_f = 2\pi/k_f$ is the Fermi wavelength and $E = \hbar k_f v_f$) with $V_0 = 200$ meV, $E_g = -0.4$ eV for (a) $\theta_k = 1^\circ$ and (b) $\theta_k = 60^\circ$ (c) $\theta_k = 120^\circ$, (d) $\theta_k = 179^\circ$. The cyan, blue, and red solid lines indicate step potential, single barrier with width $D = 3 \mu\text{m}$ and double barriers with $L = 4 \mu\text{m}$, widths $D = 3 \mu\text{m}$ respectively.

to see the resonances for $2q_y D = n\pi$ where n is an integer number. In Fig. 2 the free parameters such as separation distance, width, and V_0 are chosen in a way that the condition $2q_y D = n\pi$ is not fulfilled and therefore there are no resonances for the cases of a single and double barrier.

Let us now study how the G-H shifts are influenced by transmission resonances. Fig. 3 shows the transmissions and G-H shifts as a function of the energy for different incident angles and for different kinds of potential barriers. As already mentioned above, for single and double barriers the transmission exhibits a series of resonances at $2q_y D = n\pi$. These barriers also exhibit peaks for G-H shifts that are absent in the step potential. An important feature of these results is that around the peaks for the G-H shifts, the magnitude of transmission changes significantly. Additionally, the G-H shift through the single and double barriers shows clear resonances at $\theta_k = 1^\circ$ and $\theta_k = 179^\circ$, which can be promising candidates for the realization of G-H shift. Therefore, we can see that a G-H shift enhancement is obtained at resonant conditions for the transmission coefficient as it has been documented in graphene-based systems [68,86,87]. Our results indicate that the G-H effect is enhanced for the double barrier at high-energy and for resonant conditions. Here we are choosing $D \sim L$ in such a way that there is a strong interaction between both barriers, as if $L \rightarrow \infty$ the effect will be simply the sum of the contributions from each barrier.

To have a better understanding of transmission resonances and the G-H shifts, now we consider specific values of the barriers width. In Fig. 4 we present the transmission probability and G-H shifts (S/λ_f) for a single barrier and double barriers as a function of the barrier width for $\theta_k = 1^\circ$. This plot is consistent with previous figures in the sense that the G-H shifts can be strongly enhanced by resonances on the transmissions. In particular, electronic wave packets between the barrier can interfere constructively by increasing the barrier width, leading to an enhanced G-H shift.

In particular, these results illustrate that we enhance the magnitude of G-H shifts by considering two barriers and tuning the energy and width of barriers. By adjusting the width of the barriers, the wavelength of the charge carriers can be aligned with the distance between the barriers, leading to the occurrence of Fabry-Pérot resonances. Note that the number of resonances is the same for both the single and double barriers. Furthermore, in the case of a particle traversing a potential barrier with a near-parallel trajectory at the boundary, significant G-H shifts can arise, exhibiting potent resonances coinciding with energy and barrier width values that correspond to transmission peaks.

Studying the electronic G-H shifts in phosphorene in comparison to graphene aims to explore and comprehend the distinctions in their electronic behaviors and potential applications in nanoelectronic and

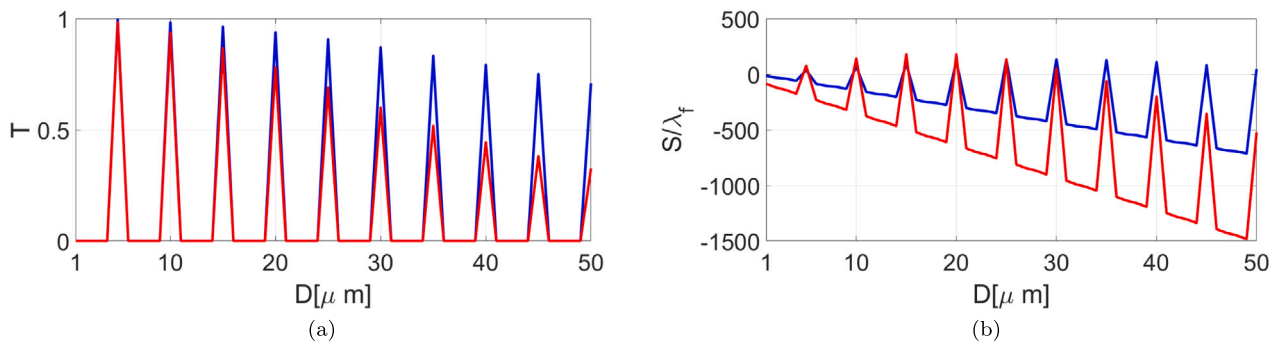


Fig. 4. Panel (a), transmission probability (T) and, panel b) G-H shifts (S/λ_f), both as the function of the barrier width D . The plots were made for incident quasiparticles with positive energy $E = 72$ meV with $V_0 = 200$ meV, $E_g = -0.4$ eV and $\theta_k = 1^\circ$. The blue curves indicate a single barrier and the red curves the case of the double barrier with $L = 4$ μm .

optoelectronic devices. As we already mentioned, the Hamiltonians of phosphorene and graphene under strong uniaxial strain are similar. Strain engineering in graphene offers the ability to modify its electronic and mechanical properties. However, applying very strong uniaxial strain can compromise the structural stability of graphene and lead to the formation of defects [48]. Overall, exploring the Electronic G-H shifts in phosphorene and comparing them with graphene offers valuable insights into the distinctive electronic properties of these two-dimensional materials.

4. Conclusion

In this paper, we have studied the influence of different kinds of barriers on the G-H shifts and transport properties of phosphorene along the armchair direction. We performed an analysis of G-H shifts for the Schrödinger and Dirac electrons, as the Hamiltonian of phosphorene is a combination of the Dirac and Schrodinger model. Importantly, we included a consideration of the hermiticity breaking of effective envelope theories at sharp boundaries, a point that was not discussed on previous efforts concerning similar systems [68,86,87]. Our results indicate that is safe to work with the usual theory of just matching the wavefunctions and derivatives at the boundary as no rotation of pseudospin is produced. This allows to dismiss the use of extra parameters to ensure current conservation and further validate previous works [68,86,87].

For normal incidence, a Klein tunneling is observed for the three types of studied barriers. Notice that the G-H shifts at the normal incidence are absent due to the constant transmission of a Dirac electron through the barrier. Our results, in general, demonstrate that the G-H shift exhibits a clear resonant behavior for the case of Schrodinger electrons, i.e., when the incidence is not normal. Thus, the G-H shift is in fact a good tool to identify some kinds of effective flavor quasiparticles.

Our calculations also show that by using single and double barriers, we have significant peaks for the G-H shift, for example at $\theta_k = 1^\circ$ and 179° , which are promising candidates for the realization of the G-H shift. The obtained results can be readily extended to extremely anisotropic strained graphene as the Hamiltonian is similar. In spite of this, the G-H effect in phosphorene is easier to observe experimentally than in graphene as such kind of extreme strain is difficult to obtain in graphene, as defects and other effects appear, like many body interactions.

CRedit authorship contribution statement

Parisa Majari: Methodology, Writing, Drafting, Revising. **Gerardo G. Naumis:** Methodology, Drafting, Revising.

Declaration of competing interest

The authors declare that they have no known competing financial interests or personal relationships that could have appeared to influence the work reported in this paper.

Data availability

No data was used for the research described in the article.

Acknowledgments

P.M. gratefully acknowledges a fellowship from CONACYT, Mexico Project Fronteras 425854, UNAM-DGAPA PAPIIT IN113620, UNAM-DGAPA PAPIIT IG101122, UNAM-PAPIIT IN102620 and CONACYT, Mexico Project 254515.

References

- [1] S. Bittner, B. Dietz, M. Miski-Oglu, P.O. Iriarte, A. Richter, F. Schäfer, *Phys. Rev. B* 82 (1) (2010) 014301.
- [2] T. Stegmann, J.A. Franco-Villafane, U. Kuhl, F. Mortessagne, T.H. Seligman, *Phys. Rev. B* 95 (3) (2017) 035413.
- [3] E. Sadurni, T.H. Seligman, F. Mortessagne, *New J. Phys.* 12 (5) (2010) 053014.
- [4] T. Stegmann, N. Szpak, *New J. Phys.* 18 (5) (2016) 053016.
- [5] Y. Betancur-Ocampo, *J. Phys.: Condens. Matter* 30 (43) (2018) 435302.
- [6] Z. Ma, Z. Chen, J. Xu, W. Li, L. Zhang, L. Wang, *Sci. Rep.* 10 (1) (2020) 1–8.
- [7] P.A. Pantaleón, V.T. Phong, G.G. Naumis, F. Guinea, *Phys. Rev. B* 106 (16) (2022) L161101.
- [8] P. Majari, *J. Phys.: Condens. Matter* 34 (26) (2022) 265401.
- [9] G.G. Naumis, *Rev. Mex. Fis.* 67 (2021) 050102 1–.
- [10] L.A. Navarro-Labastida, G.G. Naumis, *Rev. Mex. Fis.* 69 (2023) 041602 1–.
- [11] T. Mueller, F. Xia, P. Avouris, *Nat Photonics* 4 (5) (2010) 297–301.
- [12] J. Qu, H. Pan, Y.-Z. Sun, H.-F. Zhang, *Ann. Phys.* 534 (9) (2022) 2200175.
- [13] S.-W. Ng, N. Noor, Z. Zheng, *NPG Asia Mater.* 10 (4) (2018) 217–237.
- [14] J. Sui, R. Dong, S. Liao, Z. Zhao, Y. Wang, H.-F. Zhang, *Ann. Phys.* 535 (3) (2023) 2200509.
- [15] S. Guo, C. Hu, H. Zhang, *J. Opt. Soc. Amer. B* 37 (9) (2020) 2678–2687.
- [16] A. Dolatabady, N. Granpayeh, *IEEE Trans. Magn.* 54 (2) (2018) 1–5.
- [17] J.-Y. Sui, S.-y. Liao, B. Li, H.-F. Zhang, *Opt. Lett.* 47 (23) (2022) 6065–6068.
- [18] K.S. Novoselov, A.K. Geim, S.V. Morozov, D.-e. Jiang, Y. Zhang, S.V. Dubonos, I.V. Grigorieva, A.A. Firsov, *Science* 306 (5696) (2004) 666–669.
- [19] A.C. Neto, F. Guinea, N.M. Peres, K.S. Novoselov, A.K. Geim, *Rev. Modern Phys.* 81 (1) (2009) 109.
- [20] E. Munoz, J. Lu, B.I. Yakobson, *Nano Lett.* 10 (5) (2010) 1652–1656.
- [21] M. Katsnelson, K. Novoselov, A. Geim, *Nat. Phys.* 2 (9) (2006) 620–625.
- [22] V.V. Cheianov, V.I. Fal'ko, *Phys. Rev. B* 74 (4) (2006) 041403.
- [23] A.V. Shytov, M.S. Rudner, L.S. Levitov, *Phys. Rev. Lett.* 101 (15) (2008) 156804.
- [24] G.G. Naumis, S. Barraza-Lopez, M. Oliva-Leyva, H. Terrones, *Rep. Progr. Phys.* 80 (9) (2017) 096501.
- [25] M.Y. Han, B. Özyilmaz, Y. Zhang, P. Kim, *Phys. Rev. Lett.* 98 (20) (2007) 206805.
- [26] R. Garg, N.K. Dutta, N. Roy Choudhury, *Nanomaterials* 4 (2) (2014) 267–300.
- [27] R. Carrillo-Bastos, G.G. Naumis, *Phys. Status Solidi* 12 (9) (2018) 1800072.
- [28] H. Falomir, E. Muñoz, M. Loewe, R. Zamora, *J. Phys. A* 53 (1) (2019) 015401.
- [29] L. Dell'Anna, P. Majari, M. Setare, *J. Phys.: Condens. Matter* 30 (41) (2018) 415301.

- [30] A. Carvalho, M. Wang, X. Zhu, A.S. Rodin, H. Su, A.H. Castro Neto, *Nat. Rev. Mater.* 1 (11) (2016) 1–16.
- [31] M. Batmunkh, M. Bat-Erdene, J.G. Shapter, *Adv. Mater.* 28 (39) (2016) 8586–8617.
- [32] E.S. Reich, et al., *Nature* 506 (7486) (2014) 19.
- [33] L. Kou, C. Chen, S.C. Smith, *J. Phys. Chem. Lett.* 6 (14) (2015) 2794–2805.
- [34] R. Ma, S. Liu, M. Deng, L. Sheng, D. Xing, D. Sheng, *Phys. Rev. B* 97 (7) (2018) 075407.
- [35] M. Zare, B.Z. Rameshti, F.G. Ghamsari, R. Asgari, *Phys. Rev. B* 95 (4) (2017) 045422.
- [36] Y. Aierken, O. Leenaerts, F.M. Peeters, *Phys. Rev. B* 92 (10) (2015) 104104.
- [37] Q. Peng, Z. Wang, B. Sa, B. Wu, Z. Sun, *Sci. Rep.* 6 (1) (2016) 31994.
- [38] Y. Cai, G. Zhang, Y.-W. Zhang, *Sci. Rep.* 4 (1) (2014) 6677.
- [39] S. Fukuoka, T. Taen, T. Osada, *J. Phys. Soc. Japan* 84 (12) (2015) 121004.
- [40] M. Akhtar, G. Anderson, R. Zhao, A. Alruqi, J.E. Mroczkowska, G. Sumanasekera, J.B. Jasinski, *npj 2D Mater. Appl.* 1 (1) (2017) 1–13.
- [41] E.T. Sisakht, F. Fazileh, M. Zare, M. Zarenia, F. Peeters, *Phys. Rev. B* 94 (8) (2016) 085417.
- [42] T. Wang, Y. Liu, Q. Guo, B. Zhang, K. Sheng, C. Li, Y. Yin, *J. Korean Phys. Soc.* 66 (2015) 1031–1034.
- [43] M. Yarmohammadi, B.D. Hoi, L.T.T. Phuong, *Sci. Rep.* 11 (1) (2021) 3716.
- [44] D. Boukhalov, A. Rudenko, D. Prishchenko, V. Mazurenko, M. Katsnelson, *Phys. Chem. Chem. Phys.* 17 (23) (2015) 15209–15217.
- [45] L.-J. Kong, G.-H. Liu, Y.-J. Zhang, *RSC Adv.* 6 (13) (2016) 10919–10929.
- [46] H. Bui, L.T. Phuong, M. Yarmohammadi, *Europhys. Lett.* 124 (2) (2018) 27001.
- [47] D. Bui, M. Yarmohammadi, *Phys. Lett. A* 382 (28) (2018) 1885–1889.
- [48] G.G. Naumis, S. Barraza-Lopez, M. Oliva-Leyva, H. Terrones, *Rep. Progr. Phys.* 80 (9) (2017) 096501.
- [49] X. Peng, Q. Wei, A. Copple, *Phys. Rev. B* 90 (8) (2014) 085402.
- [50] S.H. Mir, S.B. Pillai, N.N. Som, P.C. Jha, P.K. Jha, *Adv. Mater. Res.* 1141 (2016) 210–214.
- [51] V. Wang, Y. Kawazoe, W. Geng, *Phys. Rev. B* 91 (4) (2015) 045433.
- [52] E. Kutlu, P. Narin, S. Lisesivdin, E. Ozbay, *Phil. Mag.* 98 (2) (2018) 155–164.
- [53] Z. Li, T. Cao, M. Wu, S.G. Louie, *Nano Lett.* 17 (4) (2017) 2280–2286.
- [54] J. Seffadi, I. Redouani, Y. Zahidi, A. Jellal, *Solid State Commun.* 351 (2022) 114777.
- [55] Y. Betancur-Ocampo, E. Paredes-Rocha, T. Stegmann, *J. Appl. Phys.* 128 (11) (2020) 114303.
- [56] Y. Betancur-Ocampo, F. Leyvraz, T. Stegmann, *Nano Lett.* 19 (11) (2019) 7760–7769.
- [57] S. Adhikary, S. Mohakud, S. Dutta, *physica status solidi (b)* 258 (10) (2021) 2100071.
- [58] S.G. y García, T. Stegmann, Y. Betancur-Ocampo, *Phys. Rev. B* 105 (12) (2022) 125139.
- [59] Y.W. Choi, H.J. Choi, *2D Mater.* 8 (3) (2021) 035024.
- [60] E. Paredes-Rocha, Y. Betancur-Ocampo, N. Szpak, T. Stegmann, *Phys. Rev. B* 103 (4) (2021) 045404.
- [61] E. Andrade, R. Carrillo-Bastos, M.M. Asmar, G.G. Naumis, *Phys. Rev. B* 106 (2022) 195413.
- [62] L. Lambrechts, V. Ginis, J. Danckaert, P. Tassin, *Metamaterials X*, Vol. 9883, SPIE, 2016, pp. 149–155.
- [63] Y. Xu, C.T. Chan, H. Chen, *Sci. Rep.* 5 (1) (2015) 1–5.
- [64] J. Wen, J. Zhang, L.-G. Wang, S.-Y. Zhu, *J. Opt. Soc. Amer. B* 34 (11) (2017) 2310–2316.
- [65] N. Ali, W.I. Waseer, Q. Naqvi, et al., *Opt. Commun.* 501 (2021) 127348.
- [66] M. Jamshidnejad, M. Jabbari, E.A. Sangachin, G. Solookinejad, *Laser Phys.* 27 (8) (2017) 085201.
- [67] D.-K. Li, S.-Y. Wang, X.-Q. Yan, B.-W. Su, Z. Hu, Z.-B. Liu, J.-G. Tian, *Appl. Phys. Lett.* 120 (5) (2022) 053105.
- [68] X. Chen, J.-W. Tao, Y. Ban, *Eur. Phys. J. B* 79 (2) (2011) 203–208.
- [69] A. Jellal, I. Redouani, Y. Zahidi, H. Bahlouli, *Physica E* 58 (2014) 30–37.
- [70] Z.-Z. Cao, Y.-F. Cheng, G.-Q. Li, *Physica B* 407 (21) (2012) 4254–4257.
- [71] Y. Liu, Z.-M. Yu, H. Jiang, S.A. Yang, *Phys. Rev. B* 98 (7) (2018) 075151.
- [72] X. Li, P. Wang, F. Xing, X.-D. Chen, Z.-B. Liu, J.-G. Tian, *Opt. Lett.* 39 (19) (2014) 5574–5577.
- [73] S. Chen, C. Mi, L. Cai, M. Liu, H. Luo, S. Wen, *Appl. Phys. Lett.* 110 (3) (2017).
- [74] N. Goyal, N. Kaushik, H. Jawa, S. Lodha, 2017 75th Annual Device Research Conference, DRC, IEEE, 2017, pp. 1–3.
- [75] J. Xiao, M. Long, X. Zhang, J. Ouyang, H. Xu, Y. Gao, *Sci. Rep.* 5 (1) (2015) 9961.
- [76] Q. Wu, L. Shen, M. Yang, Y. Cai, Z. Huang, Y.P. Feng, et al., *Phys. Rev. B* 92 (3) (2015) 035436.
- [77] V. Tran, L. Yang, *Phys. Rev. B* 89 (24) (2014) 245407.
- [78] K. Ghasemian, M. Setare, D. Jahani, *Physica E* 140 (2022) 115167.
- [79] M. Setare, P. Majari, C. Noh, S. Dehdashti, *J. Modern Opt.* 66 (16) (2019) 1663–1667.
- [80] P. Roman-Taboada, G.G. Naumis, *Phys. Rev. B* 90 (2014) 195435.
- [81] G. Bonneau, J. Faraut, G. Valent, *Am. J. Phys.* 69 (3) (2001) 322–331.
- [82] E. McCann, V.I. Fal'ko, *J. Phys.: Condens. Matter* 16 (13) (2004) 2371.
- [83] D.J. Alspaugh, M.M. Asmar, D.E. Sheehy, I. Vekhter, *Phys. Rev. B* 105 (5) (2022) 054502.
- [84] F.G. Montoya, C. Jung, T.H. Seligman, *Commun. Nonlinear Sci. Numer. Simul.* (2023) 107373.
- [85] F. Calogero, *Nonlinear Phenomena: Proceedings of the CIFMO School and Workshop, Oaxtepec, Springer, 2005*, pp. 47–109.
- [86] M. Mekkaoui, Y. Fattasse, A. Jellal, *Phys. Lett. A* 439 (2022) 128136.
- [87] Y. Chen, Y. Ban, Q.-B. Zhu, X. Chen, *Opt. Lett.* 41 (19) (2016) 4468–4471.